Orbital superconductivity, defects, and pinned nematic fluctuations in the doped iron chalcogenide $FeSe_{0.45}Te_{0.55}$

Saheli Sarkar,[1] John Van Dyke,[1,2] Peter O. Sprau,[3,4] Freek Massee,[3,4,5] Ulrich Welp,[6]
Wai-Kwong Kwok,[6] J. C. Seamus Davis,[3,7,8,9] and Dirk K. Morr[1]

[1]*Department of Physics, University of Illinois at Chicago, Chicago, Illinois 60607, USA*

[2]*Department of Physics and Astronomy, Iowa State University, Ames, Iowa 50011, USA*

[3]*LASSP, Department of Physics, Cornell University, Ithaca, New York 14853, USA*

[4]*CMPMS Department, Brookhaven National Laboratory, Upton, New York 11973, USA*

[5]*Laboratoire de Physique des Solides (CNRS UMR 8502), Bâtiment 510, Université Paris-Sud/Université Paris-Saclay, 91405 Orsay, France*

[6]*Materials Science Division Argonne National Laboratory, Argonne, Illinois 60439, USA*

[7]*MPMS Department, Brookhaven National Laboratory, Upton, New York 11973, USA*

[8]*School of Physics and Astronomy, University of St. Andrews, Fife KY16 9SS, Scotland, United Kingdom*

[9]*Tyndall National Institute, University College Cork, Cork T12R5C, Ireland*

We demonstrate that the differential conductance, dI/dV, measured via spectroscopic imaging scanning tunneling microscopy in the doped iron chalcogenide $FeSe_{0.45}Te_{0.55}$, possesses a series of characteristic features that allow one to extract the orbital structure of the superconducting gaps. This yields nearly isotropic superconducting gaps on the two holelike Fermi surfaces, and a strongly anisotropic gap on the electronlike Fermi surface. Moreover, we show that the pinning of nematic fluctuations by defects can give rise to a dumbbell-like spatial structure of the induced impurity bound states, and explains the related C_2 symmetry in the Fourier transformed differential conductance.

Identifying the electronic structure of the iron-based superconductors has remained one of the most important open challenges in determining the underlying superconducting pairing mechanism. There exists strong evidence for an $s_{\pm}$-wave symmetry of the superconducting order parameter [1,2], arising from the pairing between electronlike and holelike Fermi surface pockets that is mediated by magnetic fluctuations [3–6]. However, the existence of nematicity in the iron chalcogenide superconductor FeSe [7], and the observation of high temperature superconductivity in iron chalcogenides without hole pockets [8–10], has recently cast doubt on such a simple picture, giving rise to the proposal of orbital selective superconducting pairing [11–14]. Moreover, recent scanning tunneling spectroscopy experiments [15] have reported that even outside the nematic phase in doped $FeSe_{0.4}Te_{0.6}$, the electronic C_4 symmetry is broken, leading to an approximate C_2 symmetry in the Fourier transformed differential conductance. Whether such a symmetry breaking arises from the pinning of dynamic nematic fluctuations, or from orbital selective Mottness, is presently unclear.

In this Rapid Communication, we provide insight into these open questions by analyzing the results of spectroscopic imaging scanning tunneling microscopy (STM) experiments in the doped iron chalcogenide $FeSe_{0.45}Te_{0.55}$. In particular, we demonstrate that the differential conductance, dI/dV, possesses a series of characteristic features that allows us to extract not only the orbital structure of the superconducting order parameter, but also its momentum dependence along the three Fermi surface sheets, yielding two nearly isotropic superconducting gaps for the holelike Fermi surfaces, and a highly anisotropic gap for the electronlike Fermi surface. Moreover, we show that the pinning of nematic fluctuations gives rise to the experimentally observed dumbbell-like spatial structure of the induced impurity states, and leads to the nearly

C_2 symmetric Fourier transformed differential conductance observed experimentally [15].

Starting point for the analysis of the differential conductance, dI/dV, measured in the superconducting state of $FeSe_{0.45}Te_{0.55}$, is a five-orbital, tight-binding Hamiltonian $H = H_0 + H_{SC}$ [6], which in real space is given by

$$H_0 = -\sum_{\mathbf{r},\mathbf{r}',\sigma} \sum_{\alpha,\beta=1}^{5} t_{\mathbf{r},\mathbf{r}'}^{\alpha\beta} c_{\mathbf{r},\alpha,\sigma}^{\dagger} c_{\mathbf{r}',\beta,\sigma},$$

$$H_{SC} = -\sum_{\langle \mathbf{r},\mathbf{r}' \rangle} \sum_{\alpha=1}^{5} I_{\mathbf{r},\mathbf{r}'}^{\alpha} \, c_{\mathbf{r},\alpha,\uparrow}^{\dagger} c_{\mathbf{r}',\alpha,\downarrow}^{\dagger} c_{\mathbf{r},\alpha,\downarrow} c_{\mathbf{r}',\alpha,\uparrow}. \quad (1)$$

Here, $\alpha,\beta = 1,\ldots,5$ are the orbital indices corresponding to the $d_{xz}, d_{yz}, d_{x^2-y^2}, d_{xy}$, and $d_{3z^2-r^2}$ orbitals, respectively, $-t_{\mathbf{r},\mathbf{r}'}^{\alpha\beta}$ represents the electronic hopping amplitude between orbital α at site $\mathbf{r}$ and orbital β at site $\mathbf{r}'$, and $c_{\mathbf{r},\alpha,\sigma}^{\dagger}(c_{\mathbf{r},\alpha,\sigma})$ creates (annihilates) an electron with spin σ at site $\mathbf{r}$ in orbital α. To obtain a superconducting order parameter with $s_{\pm}$-wave symmetry [2,4], we take H_{SC} to describe superconducting intraorbital pairing between next-nearest-neighbor Fe sites (in the 1 Fe unit cell), with $I_{\mathbf{r},\mathbf{r}'}^{\alpha}$ being the pairing interaction. Using a mean-field decoupling of H_{SC}, we obtain

$$H_{SC}^{MF} = \sum_{\langle \mathbf{r},\mathbf{r}' \rangle} \sum_{\alpha=1}^{5} \Delta_{\alpha\alpha} c_{\mathbf{r},\alpha,\uparrow}^{\dagger} c_{\mathbf{r}',\alpha,\downarrow}^{\dagger} + \text{H.c.} \quad (2)$$

We extract the hopping amplitudes by fitting the momentum resolved band structure in the normal state of $FeSe_{0.42}Te_{0.58}$ obtained in angle-resolved photoemission spectroscopy (ARPES) experiments [16], as shown in Fig. 1(a) [their values are given in Tables I and II in Ref. [17], Sec. I]. $FeSe_{0.42}Te_{0.58}$ possesses three Fermi surface (FS) sheets, with
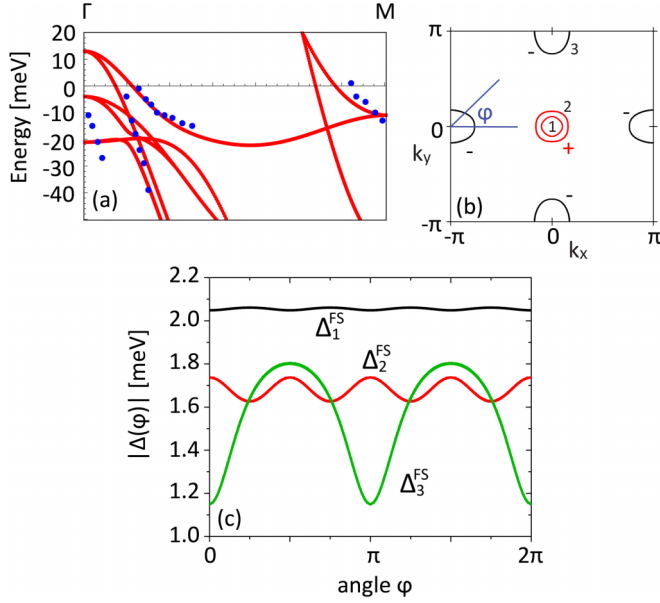
FIG. 1. (a) Theoretical fit of the experimentally determined energy dispersion of FeSe$_{0.42}$Te$_{0.58}$ [16] in the 2-Fe/cell Brillouin zone (BZ). The blue dots represent the experimentally determined dispersion [16], and the red lines represent the theoretical fit. (b) Plot of the three Fermi surface sheets resulting from the fit presented in (a) with two holelike FS pockets around the Γ [(0,0)] point and one electronlike FS pocket around the X/Y [$(\pm\pi,0),(0,\pm\pi)$] points in the 1Fe BZ. "$\pm$" indicate the phase of the superconducting $s_\pm$-wave order parameter. (c) Superconducting gap along the three Fermi surfaces as a function of angle φ measured with respect to the x axis.

two holelike FS pockets closed around the Γ point (FS 1 and 2) and one electronlike FS pocket around the X/Y points [$(\pm\pi,0),(0,\pm\pi)$] (FS 3) in the 1Fe/cell Brillouin zone [see Fig. 1(b)]. These fits reveal the orbital composition of the Fermi surfaces with states on FS 1 and 2 possessing predominant d_{xz} and d_{yz} character, while states on FS 3 possesses large contributions from the d_{xy} orbital and d_{xz}/d_{yz} orbitals (see Ref. [17], Sec. II). These results are qualitatively similar to those obtained earlier for LaOFeAs [6].

To investigate dI/dV in the superconducting state, we note that the states near the Fermi surfaces consist primarily of contributions from the d_{xz}, d_{yz}, and d_{xy} orbitals, and therefore assume that the superconducting order parameter is nonzero for these three orbitals only. To determine their values in orbital space, we make use of several characteristic features that occur in dI/dV in the superconducting state of FeSe$_{0.45}$Te$_{0.55}$, as shown in Fig. 2(a). In particular, the dI/dV lineshape possesses a set of easily identifiable coherence peaks [denoted by arrows 1 in Fig. 2(a)], located at $E = \pm 2.0$ meV, and two sets of shoulderlike features [denoted by arrows 2 and 3 in Fig. 2(a)], at energies $E = \pm 1.8$ and ± 1.2 meV, respectively. To understand the origin of these features, we plot the theoretically computed and orbitally resolved local density of states (LDOS) $N_\alpha(\mathbf{r},E)$ (see Ref. [17], Sec. I) of the d_{xz} orbital (N_{xz}) and d_{yz} orbital (N_{yz}) in Fig. 2(b), and of the d_{xy} orbital (N_{xy}) in Fig. 2(c). A plot of the total LDOS, N_{tot}, i.e., the sum over all orbital contributions, shown in Fig. 2(d), reveals that the largest contribution to N_{tot}, arises from the d_{xz}
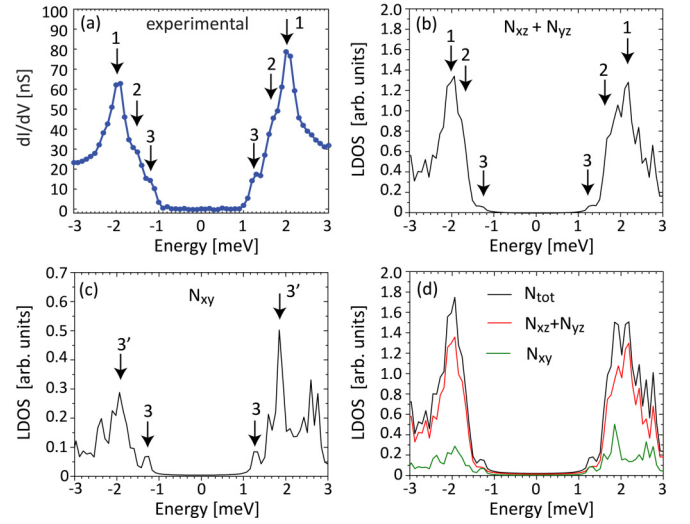
FIG. 2. (a) Experimental differential tunneling conductance $g(\mathbf{r},E = \text{eV}) = dI(\mathbf{r},V)/dV$, and theoretical (b) $N_{xz} + N_{yz}$, (c) N_{xy}, and (d) N_{tot} in FeSe$_{0.45}$Te$_{0.55}$. The sharp coherence peaks denoted by 1 are associated with the superconducting gap on Fermi surface 1, while the shoulderlike features denoted by 2 and 3 are the smeared-out coherence peaks associated with the superconducting gaps on Fermi surfaces 2 and 3. Features 3′ and 3 are features associated with the maximum and minimum superconducting gaps, $|\Delta_3|^{\text{max}}$ and $|\Delta_3|^{\text{min}}$, respectively, on Fermi surface 3.

and d_{yz} orbitals. Moreover, N_{xz} and N_{yz} [Fig. 2(b)] exhibit the same features seen experimentally: a set of coherence peaks denoted by 1, and two shoulder like features at lower energy denoted by 2 and 3. To match the energy position of these features to those observed experimentally, we take the superconducting gaps in orbital space to be given by $\Delta_{11} = \Delta_{22} = 0.55$ meV, and $\Delta_{44} = 0.38$ meV. A plot of the superconducting gaps along the three Fermi surface sheets, denoted by $\Delta_{1,2,3}^{\text{FS}}$, shown in Fig. 1(c), allows us to identify the origin of these characteristic features. In particular, the largest superconducting gap, exhibiting only a very weak variation with angle, is found on Fermi surface 1 with $\Delta_1^{\text{max}} \approx 2$ meV and gives rise to the coherence peaks denoted by arrows 1 in Fig. 2(b). The superconducting gap on Fermi surface 2, $\Delta_2^{\text{FS}}(\mathbf{k})$, exhibits a weak anisotropy and varies between $\Delta_2^{\text{min}} = 1.67$ meV and $\Delta_2^{\text{max}} = 1.73$ meV, leading to the shoulderlike feature in the LDOS indicated by arrows 2 in Fig. 2(b); this feature can be interpreted as broadened coherence peaks. Finally, the gap on Fermi surface 3 possesses the largest anisotropy varying between $|\Delta_3|^{\text{min}} = 1.2$ meV and $|\Delta_3|^{\text{max}} = 1.8$ meV, with $|\Delta_3|^{\text{min}}$ determining the position of the shoulderlike feature denoted by arrows 3. This strong anisotropy is a direct result of the varying orbital composition of states along FS 3, and a superconducting gap in the d_{xy} orbital, that is significantly smaller than that in the d_{xz} and d_{yz} orbitals (for a detailed discussion, see Ref. [17], Sec. II). Moreover, as $|\Delta_3|^{\text{max}}$ is quite close to Δ_2^{max}, it is impossible to resolve its signature in N_{xz} and N_{yz} from that of $\Delta_2^{\text{FS}}(\mathbf{k})$. However, the signatures associated with $|\Delta_3|^{\text{min}}$ and $|\Delta_3|^{\text{max}}$ can be clearly identified in N_{xy} [Fig. 2(c)] as indicated by arrows 3 and 3′. While our model assumes only two independent values of the superconducting gaps, the energies

of all three features in the theoretically computed LDOS—the coherence peaks and two shoulderlike features—are in very good agreement with the experimental findings, providing strong evidence for the validity of the extracted band structure and superconducting gaps.

The above results shed some light on the ongoing controversy regarding the size and anisotropy of the superconducting gaps reported by angle-resolved photoemission experiments on $Fe_{1.03}Te_{0.7}Se_{0.3}$ [18], $FeTe_{0.6}Se_{0.4}$ [19], and $FeTe_{0.55}Se_{0.45}$ [20]. These experiments have reported not only significantly different values of the maximum superconducting gaps, varying between 2 meV [19] and 4 meV [18,20] (with the latter being inconsistent with our results), but also disagree on whether the gaps are isotropic [18,20] or highly anisotropic [19]. In particular, the report of an isotropic superconducting gap on the electronlike Fermi surface 3 is not only inconsistent with our findings, but also with those of angle-resolved specific heat measurements [21]. The latter also reported a gap minimum on FS 3 along the $\Gamma-X/Y$ direction, in agreement with our findings.

Further important insight into the electronic structure of $FeSe_{0.45}Te_{0.55}$ can be gained by considering the experimentally measured dI/dV near defects, as shown in Fig. 3(a). Due to the unconventional symmetry of the superconducting order parameter, magnetic as well as nonmagnetic defects lead to the emergence of impurity states inside the superconducting gap [22]. These impurity states possess a dumbbell-like spatial structure [Figs. 3(c) and 3(d)], which breaks the electronic C_4 symmetry of the system, and shows little difference between the particle- ($E < 0$) and holelike ($E > 0$) branches of the defect state. The proximity to the nematic phase suggests that this dumbbell-like structure might arise from the pinning of dynamic nematic fluctuations by the defects, similar to the pinning of dynamic charge- or spin-density wave fluctuations [23]. This pinning effectively increases the spatial extent of a defect's scattering potential along the x or y axis. Alternatively, the observed broken C_4 symmetry of the defect states could reflect the presence of orbital selective Mottness [11–14].

Here, we consider the former possibility, and investigate the combined effects of defects and pinned nematic fluctuations on the electronic structure of $FeSe_{0.45}Te_{0.55}$ by employing the Hamiltonian

$$H_{\text{scat}} = U_0 \sum_{\sigma} \sum_{\alpha=1}^{5} c^{\dagger}_{\mathbf{R},\alpha,\sigma} c_{\mathbf{R},\alpha,\sigma} + U_p \Phi(\mathbf{R})$$
$$+ g \sum_{\mathbf{r},\alpha,\sigma} \Phi(\mathbf{r}) c^{\dagger}_{\mathbf{r},\alpha,\sigma} c_{\mathbf{r},\alpha,\sigma}, \quad (3)$$

where the first term describes a nonmagnetic defect located at $\mathbf{R} = (0,0)$ that leads to electronic on-site, intraorbital scattering only, the second term describes the defect-induced pinning of nematic fluctuations represented by the field $\Phi(\mathbf{R})$, and the last term represents the interaction between the nematic fluctuations and the conduction electrons with interaction strength g. The pinning of nematic fluctuations induces additional scattering potentials for the conduction electrons, described by $U_{\mathbf{r}} = g\langle\Phi(\mathbf{r})\rangle = -gU_p\chi_n(\mathbf{r}-\mathbf{R},\omega=0)$, where χ_n is the susceptibility of the nematic fluctuations. In general,
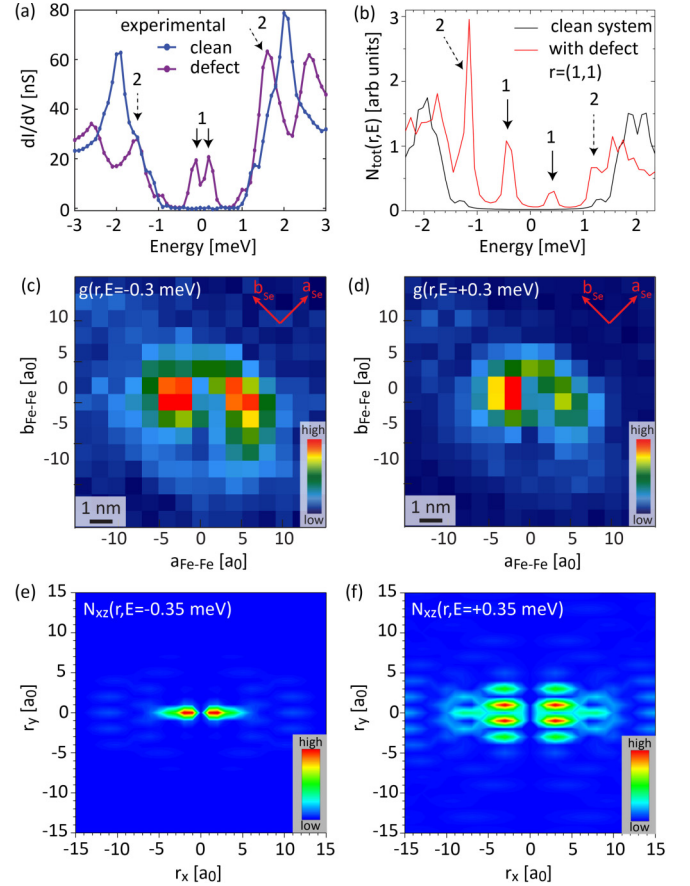
FIG. 3. (a) Experimental $dI/dV(\mathbf{r},E)$ and (b) theoretical $N_{\text{tot}}(\mathbf{r},E)$ at $\mathbf{r} = (1,1)$ with the defect located at $\mathbf{R} = (0,0)$. Experimental $dI/dV(\mathbf{r},E)$ at the (c) particlelike and (d) holelike branches of the impurity bound state. Experimental $dI/dV(\mathbf{r},E)$ was recorded at 280 mK using a modulation of 100 μV, setup bias of -20 mV, and tunneling current of 500 pA. Theoretical $N_{xz}(\mathbf{r},E)$ at the bound state energies: (e) $E_b = -0.35$ and (f) $+0.35$ meV.

the pinning of the nematic fluctuations could also affect electronic hopping elements, which will not be considered here. The spatial extent and strengths of these pinning induced scattering potentials is in general determined by the correlation lengths of the nematic fluctuations, as reflected in χ_n. While the calculation of the latter is beyond the scope of this Rapid Communnication, we make use of the fact that it is highly directional [24–27]. We therefore model the pinning of nematic fluctuations as leading to scattering potentials $U_1 = g\langle\Phi(\mathbf{R} \pm \hat{x})\rangle$ and $U_2 = g\langle\Phi(\mathbf{R} \pm 2\hat{x})\rangle$ along the x axis only. For concreteness, we use $U_0 = 100$ meV, $U_1 = 75$ meV, and $U_2 = 50$ meV for the defects considered below.

The resulting N_{tot} (see Ref. [17], Sec. I) near the defect site, shown in Fig. 3(b), reveals as expected impurity states inside the superconducting gap located at $E_b = \pm 0.35$ meV denoted by arrows 1. In addition, N_{tot} shows a strong enhancement close to the edge of the superconducting gap (denoted by arrows 2). Both of these features are in agreement with those observed experimentally [see corresponding arrows in Fig. 3(a)]. A comparison of the spatially and orbitally resolved LDOS (see Fig. S2 in Sec. III of Ref. [17]) shows that the d_{xz} orbital possesses the largest LDOS at E_b (for our choice of x and y
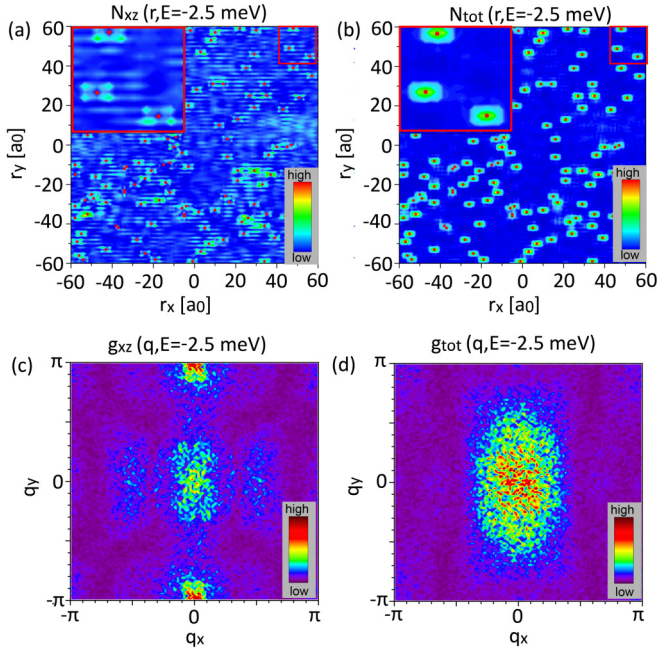
FIG. 4. Disordered system with a concentration of 1% of defects pinning nematic fluctuations and giving rise to the same scattering potentials as the defect in Fig. 3(b). Resulting theoretical (a) $N_{xz}(\mathbf{r},E)$, (b) $N_{\text{tot}}(\mathbf{r},E)$, (c) $g_{xz}(\mathbf{q},E)$, (b) $g_{\text{tot}}(\mathbf{q},E)$ at $E=-2.5$ meV.

axes and direction of nematic fluctuations). It is therefore likely that the largest contribution to the experimentally measured dI/dV at the bound state energies arises from tunneling into the d_{xz} orbitals. We therefore present in Figs. 3(e) and 3(f) the spatially resolved N_{xz} for the particle- ($E=-0.35$ meV) and holelike ($E=+0.35$ meV) branches of the defect state. Due to the pinning of the nematic fluctuations, the bound state extends primarily along the x axis, and possesses a dumbbell-like shape, similar to the one observed experimentally in Figs. 3(c) and 3(d). Note that the general spatial structure of the bound state changes only slightly between the particle- and holelike branches, in agreement with the experimental observation, and in contrast to the characteristic $45°$ rotation observed in the cuprate [28] and heavy fermion superconductors [29,30]. The reason for this striking difference lies in the orbital structure of FeSe$_{0.45}$Te$_{0.55}$: as the main contribution to the defect state resides in the d_{xz} orbital, the orbital's spatial structure restricts the bound state to predominantly lie along the x axis, and thus does not allow for a rotation of the spatial bound state pattern. Note that for a tetragonal system, nematic fluctuations both along the x and y axes are allowed, and the orientation of the dumbbells will therefore vary between the domain of nematic fluctuations they reside in.

Recent STM experiments [15] reported a breaking of the electronic C_4 symmetry, and an approximate C_2 symmetry of the Fourier transformed differential conductance, $g(\mathbf{q},E)$, outside the nematic phase in doped FeSe$_{0.4}$Te$_{0.6}$. To investigate the origin of this broken C_4 symmetry, we consider a system containing 1% of defects that pin nematic fluctuations and give rise to the same scattering potentials as the defect in Fig. 3(b)

[the defects are indicated by red dots in Figs. 4(a) and 4(b)]. We assume that the correlation length associated with the pinned nematic fluctuations is larger than the interdefect distance, such that all pinned fluctuations are aligned in the same direction. In Figs. 4(a) and 4(b), we plot the resulting $N_{xz}(\mathbf{r},E)$ and $N_{\text{tot}}(\mathbf{r},E)$, respectively, outside the superconducting gap at $E=-2.5$ meV. The zoom-in in the upper left corner of the area denoted by a red square reveals an approximate C_2 symmetry around the defects. Moreover, the defects give rise to strong spatial oscillations in $N_{xz}(\mathbf{r},E)$, possessing a wavelength of $\lambda \approx 2a_0$. By Fourier transforming $N_{xz}(\mathbf{r},E)$ and $N_{\text{tot}}(\mathbf{r},E)$, we obtain $g_{xz}(\mathbf{q},E)$ and $g_{\text{tot}}(\mathbf{q},E)$ shown in Figs. 4(c) and 4(d), respectively. As expected, they possess an approximate C_2 symmetry, and exhibit a structure that is very similar to the one observed experimentally in $g(\mathbf{q},E)$ by Singh *et al.* [15] (see Ref. [17], Sec. IV). We thus conclude that even outside the nematic phase, the pinning of strong nematic fluctuations can break the electronic C_4 symmetry of the system. The theoretical $g_{xz}(\mathbf{q},E)$ also provide insight into the origin of the strong spatial oscillations in the LDOS. The large intensity in $g_{xz}(\mathbf{q},E)$ at small wave-vectors around $(0,0)$ arises from scattering within the three Fermi surfaces, whereas the large intensity around $(0,\pm\pi)$ [see Fig. 4(c)] arises from scattering between the electronlike Fermi surface sheets closed around $(0,\pm\pi)$ and the two holelike Fermi surfaces closed around $(0,0)$ [see Fig. 1(b)]. Thus the $\lambda \approx 2a_0$ oscillations in the LDOS are a direct signature of the interband scattering induced by defects.

In conclusion, we have shown that the differential conductance, dI/dV, measured in the doped iron chalcogenide FeSe$_{0.45}$Te$_{0.55}$ provides important insight into the structure of the superconducting order parameter on three Fermi surface sheets. We extracted the magnitude and orbital content of the superconducting gaps using characteristic features in the dI/dV line shape. This allowed us to obtain nearly isotropic superconducting gaps on the two holelike Fermi surfaces, and a strongly anisotropic gap on the electronlike Fermi surface. Moreover, we demonstrated that the correlated pinning of nematic fluctuations by defects can explain not only the dumbbell-like shape of the induced impurity states, but also the broken C_4 symmetry of the observed $g(\mathbf{q},\mathbf{E})$ for energies outside the superconducting gap. Further insight into the role played by orbital-selective Mottness into determining the system's electronic structure, and response to impurities, could be provided by future experiments utilizing the yet unexplored dispersive features in the quasiparticle interference.

[1] G. R. Stewart, Rev. Mod. Phys. **83**, 1589 (2011).

[2] P. J. Hirschfeld, M. M. Korshunov, and I. I. Mazin, Rep. Prog. Phys. **74**, 124508 (2011).

[3] Q. Si, R. Yu, and E. Abrahams, Nat. Rev. Mat. **1**, 16017 (2016).

[4] I. I. Mazin, D. J. Singh, M. D. Johannes, and M. H. Du, Phys. Rev. Lett. **101**, 057003 (2008).

[5] A. V. Chubukov, D. V. Efremov, and I. Eremin, Phys. Rev. B **78**, 134512 (2008).

[6] S. Graser, T. A. Maier, P. J. Hirschfeld, and D. J. Scalapino, New J. Phys. **11**, 025016 (2009).

[7] R. M. Fernandes, A. V. Chubukov, and J. Schmalian, Nat. Phys. **10**, 97 (2014).

[8] T. Qian, X.-P. Wang, W.-C. Jin, P. Zhang, P. Richard, G. Xu, X. Dai, Z. Fang, J.-G. Guo, X.-L. Chen, and H. Ding, Phys. Rev. Lett. **106**, 187001 (2011).

[9] X. H. Niu, R. Peng, H. C. Xu, Y. J. Yan, J. Jiang, D. F. Xu, T. L. Yu, Q. Song, Z. C. Huang, Y. X. Wang, B. P. Xie, X. F. Lu, N Z. Wang, X. H. Chen, Z. Sun, and D. L. Feng, Phys. Rev. B **92**, 060504(R) (2015).

[10] L. Zhao, A. Liang, D. Yuan, Y. Hu, D. Liu, J. Huang, S. He, B. Shen, Y. Xu, X. Liu, L. Yu, G. Liu, H. Zhou, Y. Huang, X. Dong, F. Zhou, K. Liu, Z. Lu, Z. Zhao, C. Chen, Z. Xu, and X. J. Zhou, Nat. Commun. **7**, 10608 (2016).

[11] P. O. Sprau, A. Kostin, A. Kreisel, A. E. Bhmer, V. Taufour, P. C. Canfield, S. Mukherjee, P. J. Hirschfeld, B. M. Andersen, and J. C. Davis, Science **357**, 75 (2017).

[12] A. Kreisel, B. M. Andersen, P. O. Sprau, A. Kostin, J. C. Davis, and P. J. Hirschfeld, Phys. Rev. B **95**, 174504 (2017).

[13] Z. P. Yin, K. Haule, and G. Kotliar, Nat. Mat. **10**, 932 (2011).

[14] L. de Medici, G. Giovannetti, and M. Capone, Phys. Rev. Lett. **112**, 177001 (2014).

[15] U. R. Singh, S. C. White, S. Schmaus, V. Tsurkan, A. Loidl, J. Deisenhofer, and P. Wahl, Sci. Adv. **1**, e1500206 (2015).

[16] A. Tamai, A. Y. Ganin, E. Rozbicki, J. Bacsa, W. Meevasana, P. D. C. King, M. Caffio, R. Schaub, S. Margadonna, K. Prassides, M. J. Rosseinsky, and F. Baumberger, Phys. Rev. Lett. **104**, 097002 (2010).

[17] See Supplemental Material at http://link.aps.org/supplemental/10.1103/PhysRevB.96.060504 for details of the theoretical model and additional results.

[18] K. Nakayama, T. Sato, P. Richard, T. Kawahara, Y. Sekiba, T. Qian, G. F. Chen, J. L. Luo, N. L. Wang, H. Ding, and T. Takahashi, Phys. Rev. Lett. **105**, 197001 (2010).

[19] K. Okazaki, Y. Ito, Y. Ota, Y. Kotani, T. Shimojima, T. Kiss, S. Watanabe, C.-T. Chen, S. Niitaka, T. Hanaguri, H. Takagi, A. Chainani, and S. Shin, Phys. Rev. Lett. **109**, 237011 (2012).

[20] H. Miao, P. Richard, Y. Tanaka, K. Nakayama, T. Qian, K. Umezawa, T. Sato, Y.-M. Xu, Y. B. Shi, N. Xu, X.-P. Wang, P. Zhang, H.-B. Yang, Z.-J. Xu, J. S. Wen, G.-D. Gu, X. Dai, J.-P. Hu, T. Takahashi, and H. Ding, Phys. Rev. B **85**, 094506 (2012).

[21] B. Zeng, G. Mu, H. Q. Luo, T. Xiang, I. I. Mazin, H. Yang, L. Shan, C. Ren, P. C. Dai, and H.-H. Wen, Nat. Commun. **1**, 112 (2010).

[22] M. N. Gastiasoro, P. J. Hirschfeld, and B. M. Andersen, Phys. Rev. B **88**, 220509 (2013).

[23] R. H. Nyberg, E. Rossi, and D. K. Morr, Phys. Rev. B **78**, 054504 (2008).

[24] R. M. Fernandes and J. Schmalian, Supercond. Sci. Technol. **25**, 084005 (2012).

[25] R. M. Fernandes, A. V. Chubukov, J. Knolle, I. Eremin, and J. Schmalian, Phys. Rev. B **85**, 024534 (2012).

[26] Y. Wang, D. Chowdhury, and A. V. Chubukov, Phys. Rev. B **92**, 161103 (2015).

[27] U. Karahasanovic, F. Kretzschmar, T. Böhm, R. Hackl, I. Paul, Y. Gallais, and J. Schmalian, Phys. Rev. B **92**, 075134 (2015).

[28] E. W. Hudson, K. M. Lang, V. Madhavan, S. H. Pan, H. Eisaki, S. Uchida, and J. C. Davis, Nature (London) **411**, 920 (2001).

[29] B. B. Zhou, S. Misra, E. H. da Silva Neto, P. Aynajian, R. E. Baumbach, J. D. Thompson, E. D. Bauer, and A. Yazdani, Nat. Phys. **9**, 474 (2013).

[30] J. S. Van Dyke, J. C. S. Davis, and D. K. Morr, Phys. Rev. B **93**, 041107(R) (2016).